We are IntechOpen, the world's leading publisher of Open Access books Built by scientists, for scientists

6,500
Open access books available

176,000
International authors and editors

190M
Downloads

Our authors are among the

154
Countries delivered to

TOP 1%
most cited scientists

12.2%
Contributors from top 500 universities

WEB OF SCIENCE™

Selection of our books indexed in the Book Citation Index in Web of Science™ Core Collection (BKCI)

Interested in publishing with us?
Contact book.department@intechopen.com

Numbers displayed above are based on latest data collected.
For more information visit www.intechopen.com

Chapter

High-Speed Train Traction System Reliability Analysis

Kunpeng Zhang, Bin Jiang, Fuyang Chen and Hui Yang

Abstract

As the core power unit of high-speed train (HST), the diagnosis of faults in traction motor system has a significant importance on both safety and reliability, which can avoid HST crashes. According to the current problems such as early fault characteristics are not obvious and tight coupling, the reliable model with fault severity analysis and the required diagnosis accuracy cannot be achieved by current techniques. Therefore, it is crucial to evaluate HST reliability through resilience enhancement strategies to ensure it can operate with higher resilience. This chapter proposes a method for evaluating the overall reliability of HST traction motors associated with the idea of system modeling and machine learning techniques. First, a novel fault severity model is proposed suitable for the normal and fault conditions. Then electromagnetic torque energy entropy coding is utilized to extract fault features and construct different feature matrixes. Resilience enhancement strategies with support vector machine models are generated from a novel gray wolf optimizer algorithm. The performance of the proposed work is validated through simulation and experimentation on a fault-testing verification platform for the HST traction system.

Keywords: reliability analysis, high-speed train, traction motor, fault severity modeling, coupled faults, resilience enhancement

1. Introduction

Compared with other transportation means, the high-speed train (HST) has been recognized as one of the most popular tools owing to its unique advantages such as safe, comfortable and environmentally friendly. It is reported that Japan, Germany, China and France have their own HST intellectual property rights [1, 2]. On the other hand, the system performance could be severely affected by various uncertainties, such as material diversities, manufacturing tolerances and operational environment variations, resulting in a high probability of failure. As the key power equipment of HST, the resilience enhancement of the traction motor control system is essential to ensure its reliable operation. Most of the fault feature extraction and diagnosis strategies are based on the motor current signature analysis, which may cause false-negative diagnosis results in several cases [1–3]. As an alternative analysis tool, the motor's torque has been proved as the resilience enhancement method most affected by the faults during the steady-state operation [4]. In addition, the HST traction motor is a

fail-safe system with few fault samples, which makes the traditional machine learning algorithm (especially neural network) fails to the lower diagnosis accuracy associated with limited fault characteristic information [5]. In order to improve the coupled fault diagnosis, the support vector machine (SVM) classification model optimized by the gray wolf optimizer (GWO) algorithm has been proposed in [6, 7]. Though GWO has more obvious optimization power than other heuristic algorithms, the optimal local outcomes will often occur with an inflexible scheme.

It is worth noting that most of the existing works are brought forward under the assumption that only certain types of single fault may occur [8, 9]. However, in practice, coupled faults are more common to encounter in HST [1]. Considering the tight coupling components in traction motor, a single stator interturn fault may eventually lead to rotor broken bar fault [10, 11].

In general, compared with the traditional method, this paper has considered electromagnetic torque characteristics, data driven model and fault attribute knowledge coding to construct an agile fault feature matrix. Aiming at the linear indivisible attribute between fault feature and the corresponding fault classes, an improved GWO (IGWO) has been proposed to agile optimize the SVM classification model with various fault severity levels. Through the experimental analysis of the multiple fault diagnosis indexes, the advantages of the proposed reliable diagnosis approach have been proved.

2. Resilience enhancement of traction motor with coupled faults

In order to achieve resilience enhancement with high accuracy and fast speed, the empirical mode decomposition (EMD), fault coding, SVM multiclassification model and IGWO are employed in this chapter, as shown in **Figure 1**.

2.1 Fault feature extraction

For the nonlinear electromagnetic torque signals, the EMD is introduced to decompose the signal into different linear components. Then, the intrinsic mode functions (IMF) obtained from the EMD are utilized to calculate the IMF entropy, which is used to determine the fault feature matrix with the help of fault attribute knowledge coding.

2.2 Fault mechanism analysis for traction motor control system

As shown in **Figure 2**, the traction control unit achieves control of the traction motor speed and current by adjusting the gating signal of the converter at a given traction/braking command. However, the existing control units only detect faults by comparing the measured values of the sensors with the threshold values, which makes it difficult to effectively diagnose early fault (bearing fault, broken rotor bars fault, stator interturn short circuit fault, air gap eccentricity fault, rotor broken bar and interturn short circuit coupled fault). During the small fault injection phase, the traction motor current, magnetic flux and speed still satisfy the fifth-order model in the stator-side (a, b) coordinate system. Related studies have shown that the variation of parameters such as rotational inertia, rotor resistance, stator resistance and mutual inductance in the motor model can respectively describe the severity of bearing fault, broken rotor bars fault, stator interturn short circuit fault, air gap eccentricity fault.

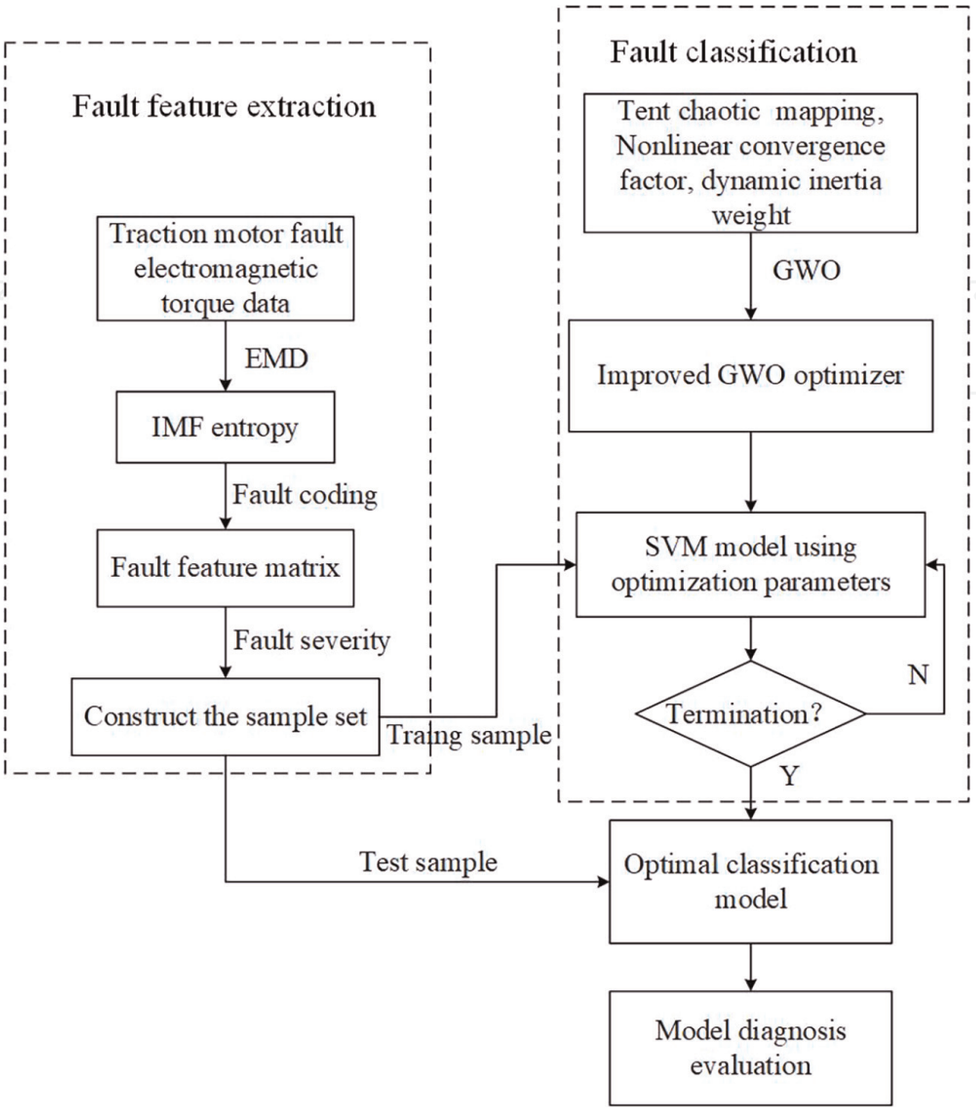

Figure 1.
Flowchart of the proposed method.

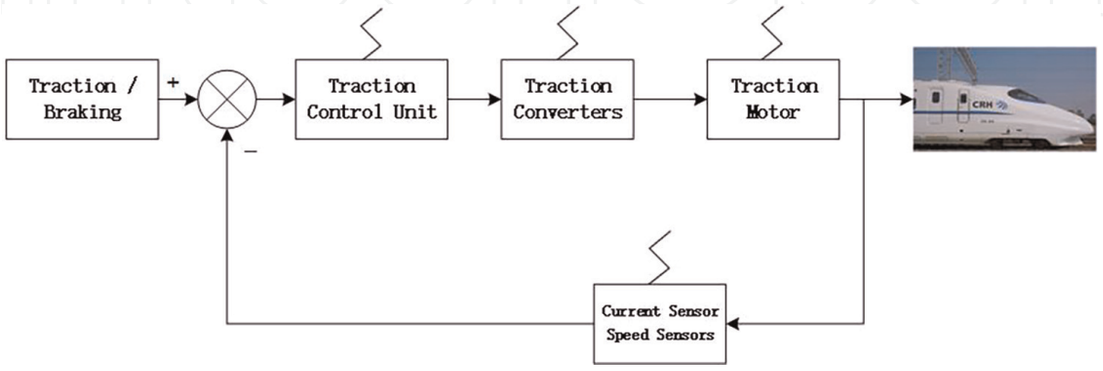

Figure 2.
High-speed train traction system.

$$
\begin{aligned}
&\frac{dw}{dt} = \frac{1}{(J+\Delta J)}(\varphi_{sa} i_{sb} - \varphi_{sb} i_{sa} - T_L) \\
&\frac{di_{sa}}{dt} = -\frac{(R_s+\Delta R_s)}{\sigma} i_{sa} - \frac{(R_r+\Delta R_r)}{L_r}(1+\vartheta(M+\Delta M)) i_{sa} \\
&\quad -\omega i_{sb} + \frac{(R_r+\Delta R_r)}{L_r \sigma}\varphi_{sa} + \frac{\omega}{\sigma}\varphi_{sb} + \frac{1}{\sigma} u_{sa} \\
&\frac{di_{sb}}{dt} = -\frac{(R_s+\Delta R_s)}{\sigma} i_{sb} - \frac{(R_r+\Delta R_r)}{L_r}(1+\vartheta(M+\Delta M)) i_{sb} \\
&-\omega i_{sa} + \frac{(R_r+\Delta R_r)}{L_r \sigma}\varphi_{sb} + \frac{\omega}{\sigma}\varphi_{sa} + \frac{1}{\sigma} u_{sb} \\
&\frac{d\varphi_{sa}}{dt} = -(R_s+\Delta R_s) i_{sa} + u_{sa} \\
&\frac{d\varphi_{sb}}{dt} = -(R_s+\Delta R_s) i_{sb} + u_{sb} \\
&T_e = \varphi_{sa} i_{sb} - \varphi_{sb} i_{sa}
\end{aligned}
\tag{1}
$$

where u_{sa} and u_{sb} are the stator side a phase and b phase voltages; i_{sa} and i_{sb} are the stator side a phase and b phase currents; φ_{sa} and φ_{sb} are the stator side a phase and b phase fluxes; w is the motor speed, J is the motor inertia, ΔJ represents the change in inertia in case of bearing fault; R_r is the rotor resistance, ΔR_r is the change in rotor resistance in case of broken rotor strip fault; R_s is the stator resistance, ΔR_s means the relative change of stator resistance; L_s, L_r and M are stator self-inductance, rotor self-inductance and mutual inductance, respectively; is the mutual inductance change during air gap eccentricity fault, T_L is the load torque; $\vartheta = \frac{M+\Delta M}{\sigma L_r}$, $\sigma = L_s\left(1 - \frac{(M+\Delta M)^2}{L_s L_r}\right)$.

From the above equation, it can be seen that the electromagnetic torque T_e contains the interaction of magnetic chain φ_{sa}, φ_{sb} and current i_{sa}, i_{sb}, and also describes the variation law of motor speed w. It is sensitive to the early motor fault variation quantities ΔJ, ΔR_r, ΔR_s and ΔM, which can best characterize the traction motor fault features. According to [10, 11], the motor early bearing fault severity η_1, broken rotor bars fault severity η_2, stator interturn short circuit fault severity η_3, air gap eccentricity fault severity η_4 can be quantified and described as follows:

$$
\begin{aligned}
\eta_1 = \frac{\Delta J}{J} \times 100\%;\ \ \eta_2 = \frac{\Delta R_r}{R_r} \times 100\% \\
\eta_3 = \frac{\Delta R_s}{R_s} \times 100\%;\ \ \eta_4 = \frac{\Delta M}{M} \times 100\%
\end{aligned}
\tag{2}
$$

2.3 Fault severity levels coding

Based on the available fault features obtained by EMD and IMF entropy, the current analysis methods often ignore the difference in fault levels. In order to make use of the distributed feature more effectively, the fault features are first coded in group mode, and then the fault feature bases that reflects various fault severity levels can be obtained. According to [12], the grouping fault features can be divided into five subblocks in terms of normal state, bearing fault, rotor broken strip, interturn short circuit and air gap eccentricity. The corresponding fault codes are described as follows:

$$\begin{cases} f_1(H_1, H_j, B_1) = \gamma_1 \\ \quad \vdots \\ f_5(H_1, H_j, B_5) = \gamma_5 \end{cases} \tag{3}$$

where $f_1, \cdots, f_5$ are the code mapping functions characterizing the motor operation conditions, $\gamma_1, \cdots, \gamma_5$ refer to the coded fault feature matrix; $B_1, \cdots, B_5$ are the five binary matrices describing the fault severity levels, which can be determined by the maintenance experience. As for B_i, the corresponding binary bits are defined in **Table 1**.

For the single fault, **Table 1** summarizes the number of potential classes is 32. Since the real fault that occurred is limited, the constructed fault coding matrix will cover 160 classes that can satisfy fault attribute transfer with various levels.

As mentioned before, the key to coding is to determine the attributes of newly extracted features only by these bases. Then, the fault feature-based agile diagnosis problem is naturally done in a classification way that transfers from training faults to target faults [13].

2.4 Gray wolf optimization algorithm

The gray wolf optimization algorithm simulates the behaviors of searching and tracking, encircling and attacking the prey based on the cooperative behavior of the gray wolf pack to achieve the purpose of optimal solution. The details are as follows:

Step 1: Social hierarchy. The gray wolf population has an extremely strict social dominance hierarchy, according to which the gray wolves can be divided into four classes, from high to low, namely α, β, δ and μ. α, β, δ are the three wolves with the best adaptation in the pack, and the remaining gray wolves are μ. The pursuit is launched by α, β, δ to perform a prey tracking roundup, and the location of the prey corresponds to the optimal global solution of the SVM parameter optimization problem.

Step 2: Surrounding the prey. When searching for prey, the gray wolf will gradually approach and then encircle, and this behavior can be expressed as:

$$\begin{cases} D = \left| Z \cdot X_p(\tau) - X(\tau) \right| \\ X(\tau + 1) = X_p(\tau) - A \cdot D \\ A = 2a \cdot r_1 - a \\ Z = 2 \cdot r_2 \end{cases} \tag{4}$$

where τ is the number of iterations, A, Z is the coefficient vectors, X_p is the position vector of the prey, X is the position vector of a gray wolf, and r_1, r_2 are random vectors in [0,1]. The value of the convergence factor a is linearly decreased from 2 to 0 as follows:

0–20%	20–30%	30–40%	40–50%	50–60%
b1	b2	b3	b4	b5

Table 1.
Binary code for fault severity levels.

$$a = 2 - 2 \cdot \frac{\tau}{T} \tag{5}$$

where T is the maximum number of iterations.

Step 3: Hunting. After encircling the prey, wolves β and δ will hunt under the leadership of wolf α. In order to simulate hunting behavior, it is assumed that α, β, δ have a better understanding of the potential location of the prey. The formula is expressed as follows:

$$\begin{cases} D_\alpha(\tau) = |Z_1 \cdot X_\alpha(\tau) - X(\tau)| \\ D_\beta(\tau) = |Z_2 \cdot X_\beta(\tau) - X(\tau)| \\ D_\delta(\tau) = |Z_3 \cdot X_\delta(\tau) - X(\tau)| \end{cases} \tag{6}$$

$$\begin{cases} X_1(\tau) = X_\alpha(\tau) - A_1 \cdot (D_\alpha(\tau)) \\ X_2(\tau) = X_\beta(\tau) - A_2 \cdot (D_\beta(\tau)) \\ X_3(\tau) = X_\delta(\tau) - A_3 \cdot (D_\delta(\tau)) \end{cases} \tag{7}$$

$$X(\tau + 1) = \frac{X_1(\tau) + X_2(\tau) + X_3(\tau)}{3} \tag{8}$$

where $D_\alpha, D_\beta, D_\delta$ denotes the distance between α, β, δ and other individuals, respectively, Z_1, Z_2, Z_3 are random vectors, $X_\alpha, X_\beta, X_\delta$ denotes the current position of α, β, δ, $X(\tau + 1)$ is the optimal solution for the current iteration.

2.5 Improved gray wolf optimization algorithm

2.5.1 Initialization strategy based on chaotic tent mapping

The traditional gray wolf algorithm solves optimization problems often based on randomness to generate initial populations, which makes the initial populations unevenly distributed and leads to a reduced speed of finding the best. In contrast, chaotic motion has the properties of randomness, regularity and ergodicity, and using these advantages can generate a better diversity of initial populations and improve the global search ability of the algorithm. The Tent mapping is as follows:

$$x_t + 1 = \begin{cases} 2x_t, 0 \le x_t \le 0.5 \\ 2(1 - x_t), 0.5 < x_t \le 1 \end{cases} \tag{9}$$

where x_t, x_{t+1} denotes the position of the t^{th} and $(t + 1)^{th}$ gray wolves in the one-dimensional space individual.

2.5.2 Adaptive adjustment strategy for control parameters

The implementation of the gray wolf algorithm mainly lies in prey localization and wolf pack movement, and the position update of individual gray wolves is influenced by the parameters. When $|A| < 1$, the wolf pack narrows the search range and conducts local search, and when $|A| > 1$, the wolf pack expands the search range and conducts global search to find a better preferred solution. The value of A in turn varies with the convergence factor a, which can balance the global and local search ability for the gray wolf algorithm. In the traditional gray wolf

optimization algorithm. Meanwhile, the parameter a varies using a linear adjustment strategy, which ignores the diversity of optimization problems to be solved and makes it difficult to reach the global optimum. In this chapter, the new convergence factor a that varies nonlinearly with the number of iterations can be described as follows:

$$a(t) = (a_{\text{initial}} - a_{\text{final}}) \cdot \left(\frac{T-\tau}{T}\right)^{\ell} \tag{10}$$

where a_{initial} is 2, a_{final} is 0, τ is the current number of iterations, T is the maximum number of iterations, ℓ is the nonlinear adjustment coefficient. In this chapter, ℓ is chosen as 0.2. At the beginning of the iteration, the a value can be reduced more slowly to increase the search range, and at the end of the iteration, the a value can be reduced faster to increase the convergence speed of the algorithm.

2.5.3 Inertia weight position update

As can be seen from Eq. (7), the traditional gray wolf algorithm position update mechanism lacks weights related to the number of iterations and is prone to fall into local optimum. In this paper, a new gray wolf position updating formula based on inertia weights, which empowers the gray wolf to jump out of local extremes, as follows:

$$\kappa(\tau) = \kappa_{\max} - (\kappa_{\max} - \kappa_{\min}) \cdot \frac{\tau}{T} \tag{11}$$

where κ is the inertia weight; $\kappa_{\max}$ denotes the maximum value of inertia weight, generally taken as 0.9; $\kappa_{\min}$ denotes the minimum value of inertia weight, generally chosen as 0.4.

2.5.4 Agile fault classification with IGWO-SVM model

For the confidence evaluation, the training sample and the test sample are constructed in the same weight. In the stage of fault classification, the tent chaotic mapping, nonlinear convergence factor and dynamic inertia weight are applied to improve GWO performances. Then, the training set will be utilized to train the SVM model. Through agile parameter optimization by IGWO, the best SVM parameter for the optimal model can be achieved.

Different from the extensively used fitness evaluated with the training set, a novel SVM classification accuracy focusing on the test set is selected to satisfy the agile diagnosis, as depicted by

$$\Gamma = \frac{1}{m}\sum_{n=1}^{m}\left(\frac{l_m}{l_n} \times 100\%\right) \tag{12}$$

where m is the number of fault class in the test set, l_m is the number of correctly identified faults in the nth test set, and l_n is the total number of samples. The optimal parameters will be utilized to build the agile fault diagnosis model.

3. Application of the proposed method

In order to verify the effectiveness of the proposed agile fault diagnosis strategy, the comparative experiments conducted on a semiphysical platform of HST traction system in CRRC Zhuzhou Locomotive Company Ltd. (see [14, 15]), are presented in this section. The fault injection benchmark platform shown in **Figure 3** includes a traction control unit, a dSPACE real-time simulator, a signal conditioner, a power source, a host computer and an operation platform.

3.1 Multiple fault injections

To obtain the validation data sets, four kinds of faults with various severity levels are injected to the dSPACE Control Desk. For the unified modeling regarding to the

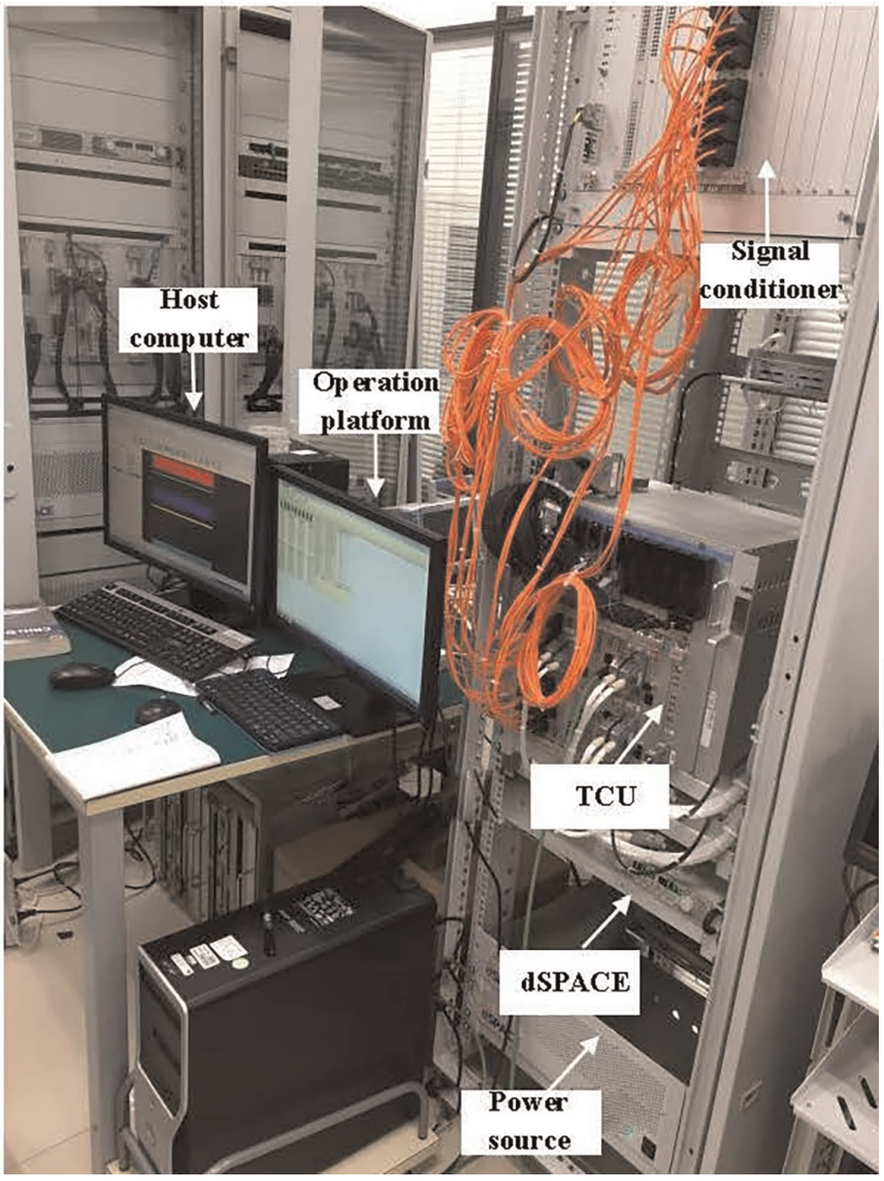

Figure 3.
HST traction system experimental setup for agile fault diagnosis.

normal and fault conditions, the experiments are executed under the steady-operation speed 110 km/h. Based on the motor model in [16], the electromagnetic torque signal sensitive to the faults can be easily reconstructed with the measurable weak current and speed signal. Considering the agile diagnosis requirements, the sampling frequency is 200 μs and the simulation time is 1 s. In order to explore the torque dynamics with various severity levels, **Figures 4–8** show the fault scenarios with a 50% ratio injecting at 0.6 s. From **Figures 4–8**, the incipient faults can be agilely detected after the fault injections, which means the torque signal is suitable for fault feature extraction and keeps consistent with the theoretical description in [17, 18].

3.2 Fault feature extraction

Based on the fault severity attribute knowledge in terms of (20–30%, 30–40%, 40–50%, and 50–60%), each group contains 5000 samples. To test the robustness of the proposed fault coding based attribute transfer method, 60 coding groups of train/test split have been collected. Then, EMD and IMF energy entropy are utilized to determine the fault feature set. By testing a large amount of the torque signal data, the

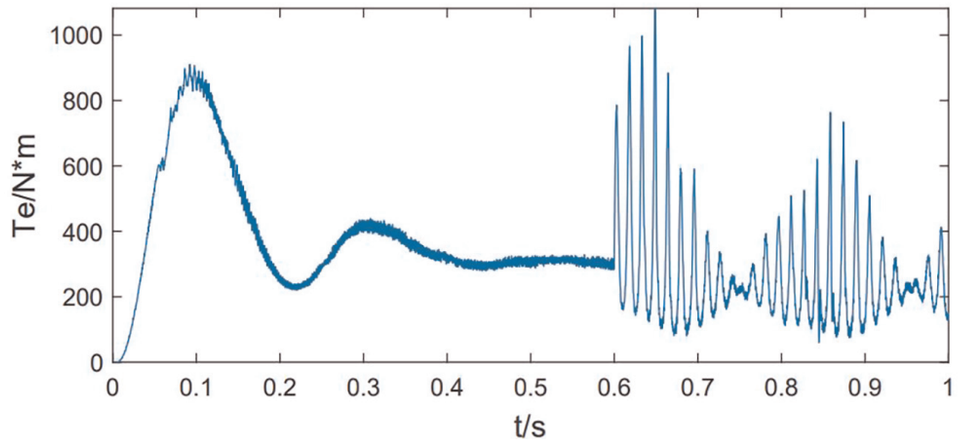

Figure 4.
Bearing fault dynamics with the electromagnetic torque signal.

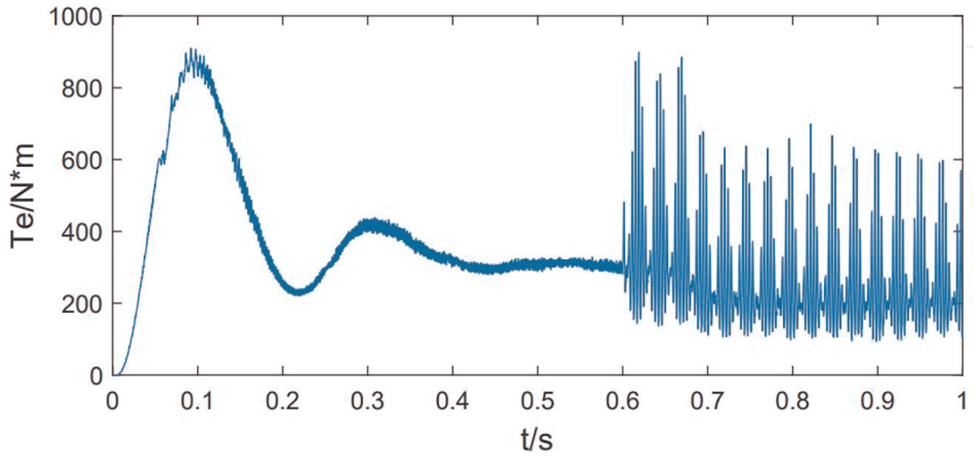

Figure 5.
Rotor fault dynamics with the electromagnetic torque signal.

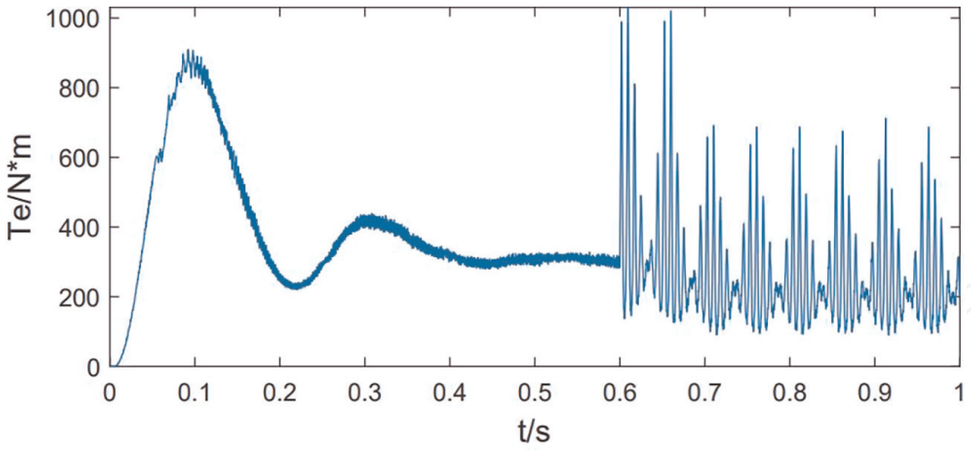

Figure 6.
Stator fault dynamics with the electromagnetic torque signal.

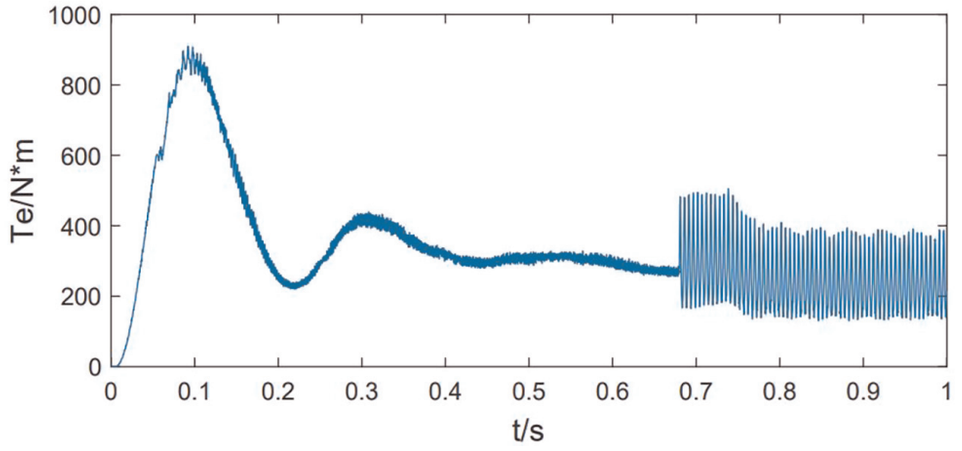

Figure 7.
Air-gap fault dynamics with the electromagnetic torque signal.

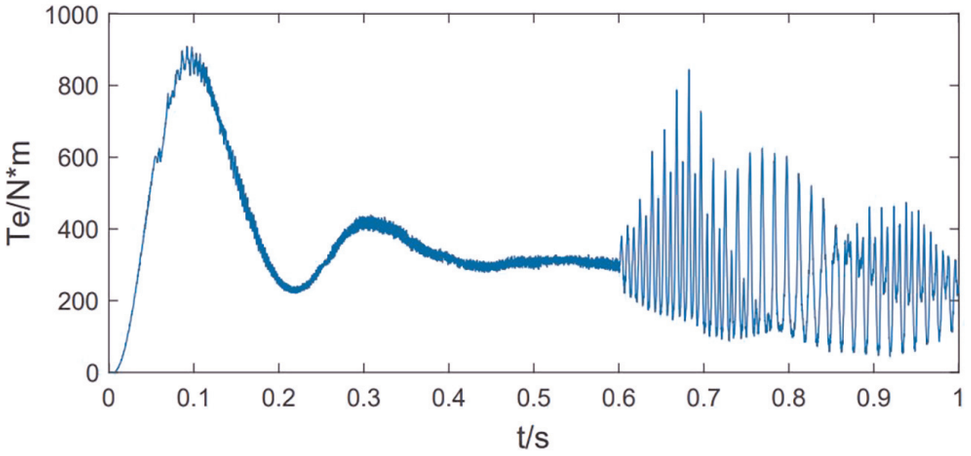

Figure 8.
Rotor and stator fault dynamics with the electromagnetic torque signal.

DOI: http://dx.doi.org/10.5772/intechopen.111911

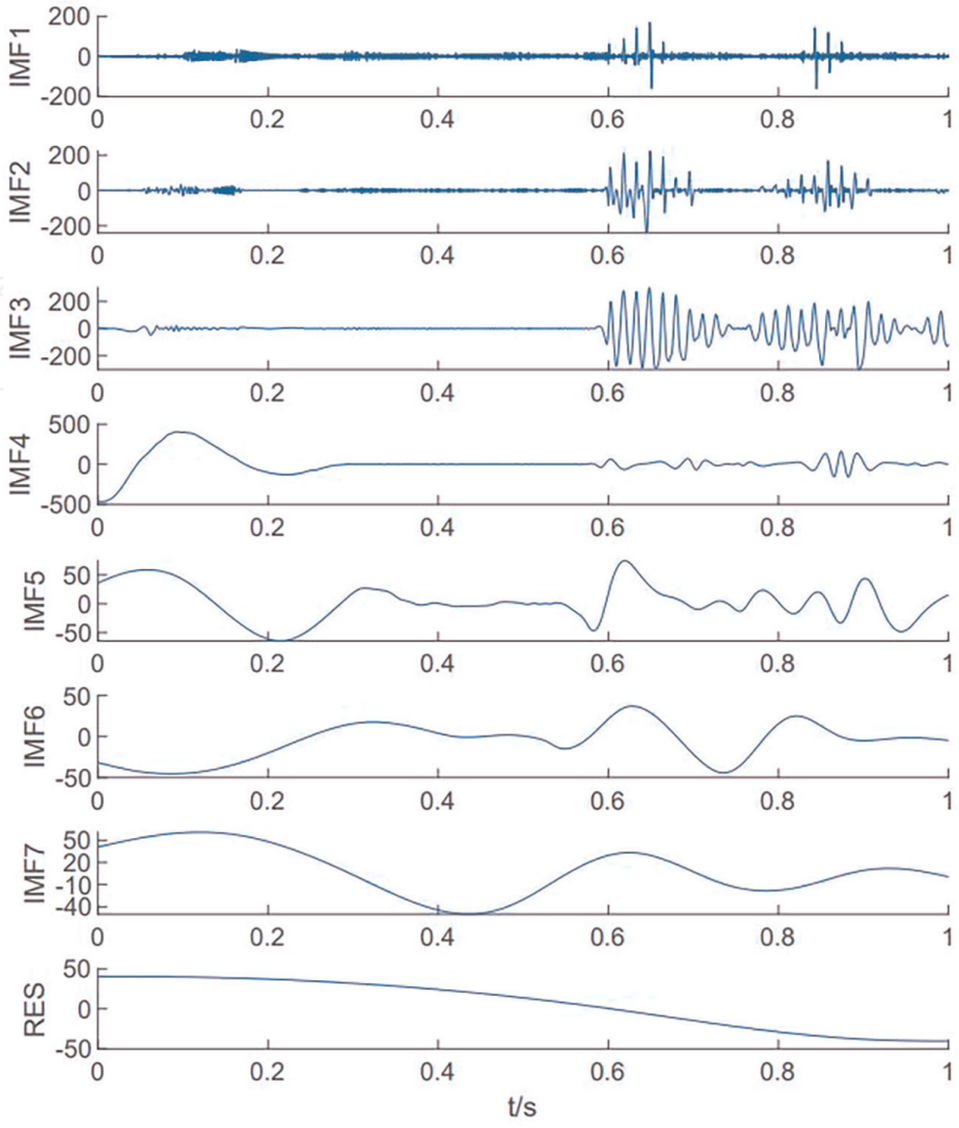

Figure 9.
The EMD of Air-gap fault signal.

default components are seven. As an example, the EMD for the electromagnetic torque signal corresponding to the air gap eccentricity fault is shown in **Figure 9**. Compared with the original signal in **Figure 4**, it can be observed that the signal part mostly lies in the first five IMFs and the dominant part of the noise exist in the sixth and seventh IMFs. Based on the coding scheme, the first five IMFs are provided in **Table 2**. **Table 2** shows that these encoded feature matrix dynamics are consistent with the fault attribute knowledge in **Table 1**. As a result, the fault attribute transfer can be achieved.

To explore the feasibility of the sharing of attribute learners, 30 coded groups in each fault mode are randomly selected to train the SVM model, and the remaining 30 groups for each fault category are treated as the test data. For the training and testing of the SVM model, fault type 1 represents the normal state while the 2, 3, 4, 5 and 6 indicate air gap eccentricity fault, stator interturn short circuit fault, broken rotor bars fault, bearing fault and compound fault, respectively. The test samples are stored in the following order: 1–30 for the normal state (label 1), 31–60 for the air gap

Motor health state	Sample Sequence	Energy entropy				
		IMF1	IMF2	IMF3	IMF4	IMF5
Normal state	1	0.00837	0.01004	0.00363	0.00277	0.36240
	2	0.00834	0.00970	0.00352	0.00260	0.36208
	...	...	...	...	...	...
	60	0.00773	0.00912	0.00313	0.00263	0.36198
Air gap eccentricity	1	0.00753	0.00878	0.02491	0.09594	0.36676
	2	0.01012	0.01168	0.03919	0.12453	0.36705
	...	...	...	...	...	...
	60	0.00333	0.32529	0.17302	0.17338	0.04985
Stator interturn short circuit fault	1	0.00991	0.11932	0.02042	0.00462	0.36679
	2	0.00836	0.12255	0.01845	0.00425	0.36672
	...	...	...	...	...	...
	60	0.00844	0.22382	0.02367	0.01362	0.36727
Broken rotor bars fault	1	0.00791	0.18749	0.34343	0.07127	0.23441
	2	0.00738	0.08977	0.28331	0.00895	0.35132
	...	...	...	...	...	...
	60	0.01037	0.21487	0.33645	0.09916	0.21056
Bearing fault	1	0.00692	0.14336	0.07425	0.00292	0.36780
	2	0.00916	0.01549	0.09111	0.00327	0.36510
	...	...	...	...	...	...
	60	0.00895	0.08748	0.12520	0.00325	0.36776
Compound faults	1	0.00723	0.01325	0.18894	0.14821	0.36479
	2	0.00908	0.02352	0.25020	0.14173	0.35896
	...	...	...	...	...	...
	60	0.00891	0.01269	0.17194	0.09948	0.36788

Table 2.
Energy entropy with various fault types.

eccentricity fault (label 2), 61–90 for the stator interturn short circuit fault (label 3), 91–120 for the broken rotor bars fault (label 4), 121–150 for the bearing fault (label 5) and 151–180 for the compound fault (label 6).

3.3 Agile fault classification

In order to achieve the agile fault classification, the comparative optimizers of GWO, particle swarm algorithm (PSO), enetic algorithm (GA) and IGWO have been employed for parameter optimization of the SVM prediction model. The four optimizer parameters are set to a population size of 20 and a number of iterations of 100. Then, the range of the SVM model parameters is set to [0.01, 100].

The four algorithms were trained with the SVM model under the training set while the test set classification accuracy (12) was used as the optimization target, and the optimal parameters obtained are shown in **Table 3**, and the adaptation curves are shown in **Figure 10**. As can be seen from **Table 3** and **Figure 10**, the fitness values corresponding to the IGWO optimized SVM parameters reach their maximum values earlier than those of GWO, PSO and GA, and the test set fault identification rate obtained by IGWO is higher than that of GWO, PSO and GA, indicating that IGWO can obtain the optimal SVM parameters quickly and accurately in the search domain than GWO, PSO and GA. In terms of convergence effect, the PSO and GA optimization algorithms obtain optimal results around 66 and 45 generations, respectively, and converge more slowly than the GWO and IGWO optimization algorithms. Comparing the GWO optimization algorithm, we can see that the IGWO and GWO algorithms have faster convergence speed, but the GWO algorithm is easy to fall into local

Diagnostic model	Best C parameter	Best σ parameter	Diagnostic accuracy
IGWO-SVM	36.78	0.227	98.89%
GWO-SVM	17.09	0.3804	98.33%
PSO-SVM	8.573	0.58	96.67%
GA-SVM	17.066	4.5231	95%

Table 3.
Parameter optimization results and fault identification rate.

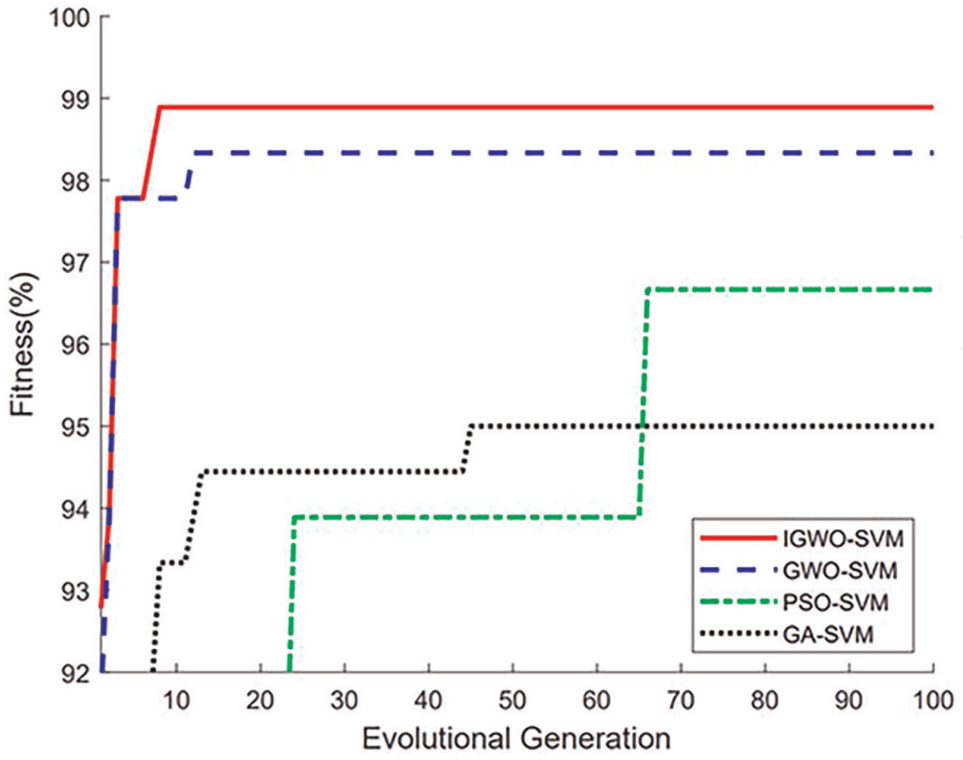

Figure 10.
Fitness curves of IGWO-SVM, GWO-SVM, PSO-SVM and GA-SVM parameter optimization process.

optimum. In summary, the IGWO-SVM classification model outperforms the other three classification models both in terms of fault recognition rate, adaptation and convergence speed.

The results of the IGWO-SVM classification model, GWO-SVM classification model, PSO-SVM classification model and GA-SVM classification model for the identification of five types of faults and normal states of the traction motor are shown in **Figures 11–14**. The hollow circle *o* indicates the actual fault category, + indicates the predicted fault category, and if the two overlap, the prediction is accurate; if not, the prediction is wrong. In the comparison experimental results, the GA-SVM classification model identified 171 groups out of 180 test samples, with an overall recognition rate of 95%, but 1 sample of category 3 (stator interturn short circuit fault) were incorrectly classified into category 2(air gap eccentricity fault), with a false alarm rate of 3.33%; 8 samples of category 6 (Coupled faults) was incorrectly classified into category 2 (air gap eccentricity fault), with a false alarm rate of 26.67%; From the above analysis, it can be seen that although GA-SVM has a high fault recognition rate, it is difficult to meet the requirement of less than 10% false alarm rate of high-speed train traction system in terms of local fault diagnosis.

The PSO-SVM classification model identified 176 groups in 180 test samples, with an overall recognition rate of 97.2%, but 1 sample of category 4 (broken rotor bars fault) was incorrectly classified into category 6(compound faults), with a false alarm rate of 3.33%; 1 sample of category 5 (bearing fault) was incorrectly classified into category 3 (stator interturn short circuit fault), with a false alarm rate of 3.33%; 4 samples of category 6 (coupled faults) was incorrectly classified into category 2 (air gap eccentricity fault), with a false alarm rate of 10%. From the comparative analysis results, it can be seen that PSO-SVM has a higher overall recognition rate compared to

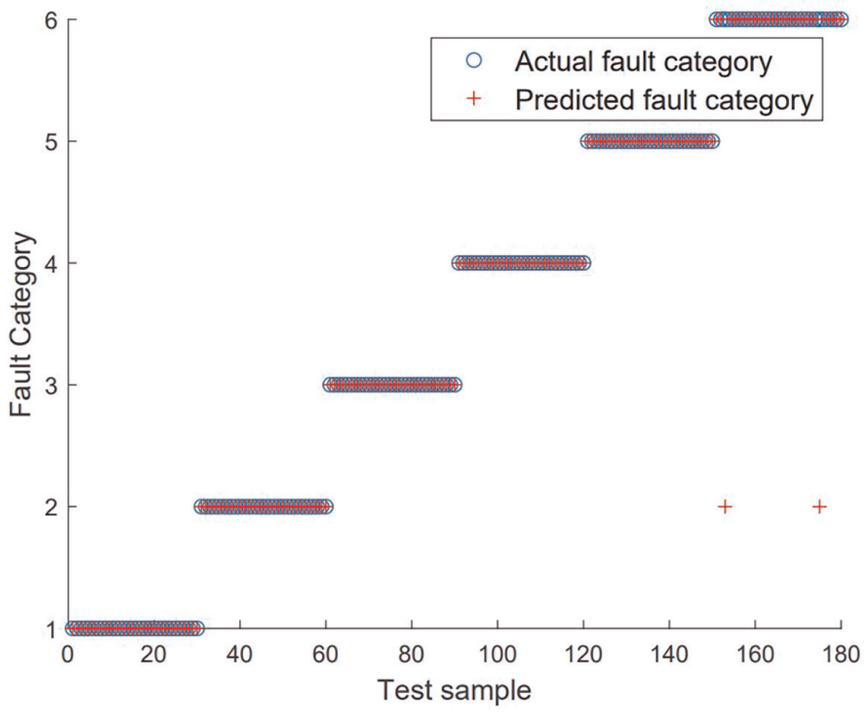

Figure 11.
Fault diagnosis result in IGWO-SVM.

DOI: http://dx.doi.org/10.5772/intechopen.111911

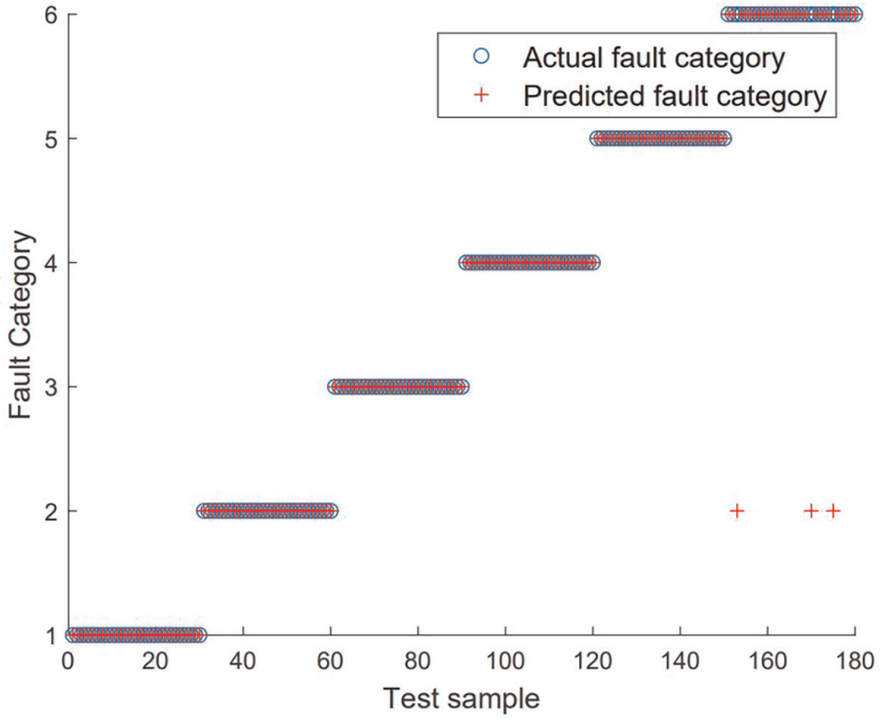

Figure 12.
Fault diagnosis result in GWO-SVM.

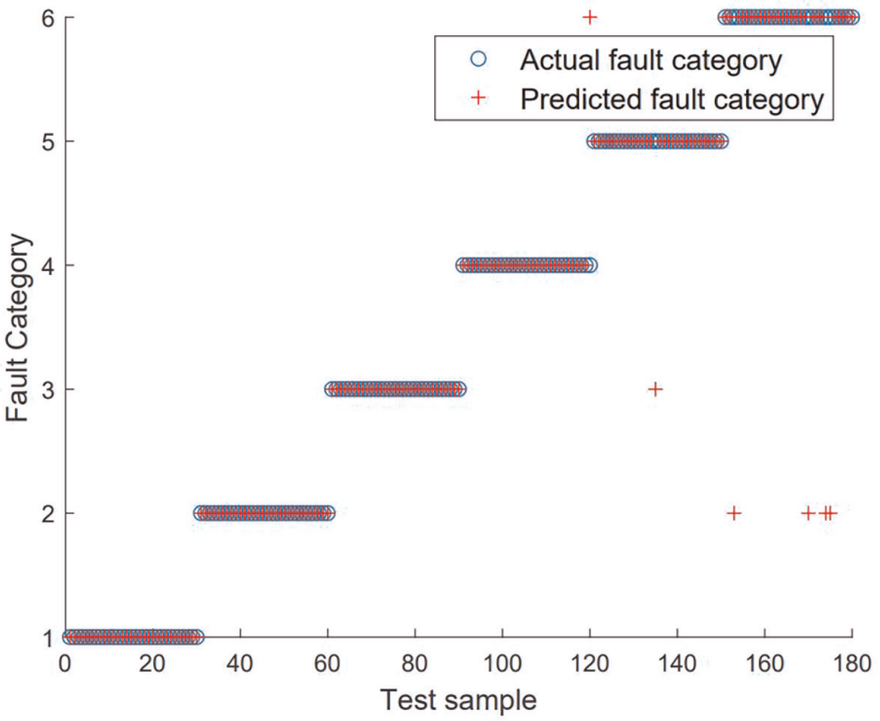

Figure 13.
Fault diagnosis result in PSO-SVM.

GA-SVM, but it is difficult to meet the requirement of less than 10% false alarm rate for high-speed train traction system faults in local fault diagnosis, especially compound faults.

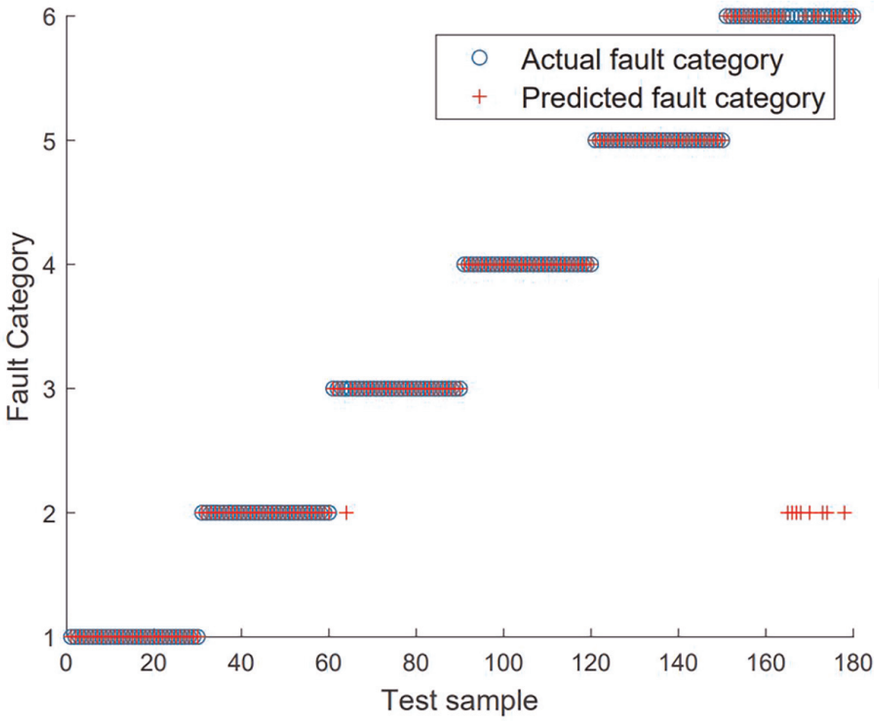

Figure 14.
Fault diagnosis result in GA-SVM.

The GWO-SVM classification model identified 177 groups out of 180 test samples, with an overall recognition rate of 98.33%. However, 1 sample of category 6 (Coupled faults) was incorrectly classified into category 2(air gap eccentricity fault), with a false alarm rate of 10%. Compared with GA-SVM and PSO-SVM, GWO-SVM has a higher overall recognition rate and also meets the requirement of less than 10% false alarm rate for high-speed train traction systems but increases the probability of misclassification of fault samples.

The SVM classification model optimized by IGWO identified 178 groups out of 180 test samples, with an overall recognition rate of 98.89%. The model only had two samples incorrectly classified into category 2 (air gap eccentricity fault) in category 6 (coupled faults), with a false alarm rate of 6.67%. The classification model proposed in this paper not only meets the requirement of less than 10% false alarm rate of high-speed train traction systems but also avoids increasing the probability of misclassification of fault samples.

4. Conclusion

1. This paper adopts a resilience enhancement strategies based on the fault severity modeling, entropy coding of electromagnetic torque energy, support vector machine classification model, and optimized fusion of improved gray wolf algorithm, which is more accurate in distinguishing small fault features and improving multi-fault diagnosis accuracy compared with other schemes.

2. Through the experiments on the data set of semiphysical simulation platform of high-speed train traction system, the results show that the proposed scheme has

certain guiding significance for traction motor fault feature extraction and accurate localization.

3. The proposed scheme can effectively diagnose the multiple fault modes of traction motors of high-speed trains and can also be applied to the identification of other equipment fault types of high-speed trains.

IntechOpen

Author details

Kunpeng Zhang[1*], Bin Jiang[2], Fuyang Chen[2] and Hui Yang[1]

1 School of Electrical and Automation Engineering, East China Jiaotong University, Nanchang, China

2 College of Automation Engineering, Nanjing University of Aeronautics and Astronautics, Nanjing, China

*Address all correspondence to: ecjtu.zhangkunpeng@163.com

IntechOpen

© 2023 The Author(s). Licensee IntechOpen. This chapter is distributed under the terms of the Creative Commons Attribution License (http://creativecommons.org/licenses/by/3.0), which permits unrestricted use, distribution, and reproduction in any medium, provided the original work is properly cited. CC BY

References

[1] Chen HT, Jiang B, Li ZH. Edge computing-aided framework of fault detection for traction control systems in high-speed trains. IEEE Transactions on Vehicular Technology. 2020;**69**(2): 1309-1318. DOI: 10.1109/TVT. 2019.2957692

[2] Kim Y, Koo B, Nam K. Induction motor design strategy for wide constant power speed range. IEEE Transactions on Industrial Electronics. 2019;**66**(11): 8372-8381. DOI: 10.1109/ TIE.2018.2885691

[3] Yang CH, Yang C, Yang XY, Gui WH. A fault-injection strategy for traction drive control systems. IEEE Transactions on Industrial Electronics. 2017;**64**(7): 5719-5727. DOI: 10.1109/TIE.2017. 2674610

[4] Zhou DH, Ji HQ, He X, Shang J. Fault detection and isolation of the brake cylinder system for electric multiple units. IEEE Transactions on Control Systems Technology. 2018;**26**(5): 1744-1757. DOI: 10.1109/ TCST.2017.2718979

[5] Prakash O, Samantaray AK, Bhattacharyya R. Model-based diagnosis of multiple faults in hybrid dynamical systems with dynamically updated parameters. IEEE Transactions on Systems, Man, and Cybernetics:Systems. 2019;**49**(6):1053-1072. DOI: 10.1109/ TSMC.2017.2710143

[6] Singh A, Grant B, Defour R, Sharma C, Bahadoorsingh S. A review of induction motor fault modeling. Electric Power Systems Research. 2016;**133**: 191-197. DOI: 10.1016/j.epsr.2015.12.017

[7] Yu WK, Zhao CH. Online fault diagnosis in industrial processes using multimodel exponential discriminant analysis algorithm. IEEE Transactions on Control Systems Technology. 2019; **27**(3):1317-1325. DOI: 10.1109/ TCST.2017.2789188

[8] Wang F, Xu TH, Tang T, Zhou MC, Wang HF. Bilevel feature extraction-based text mining for fault diagnosis of railway systems. IEEE Transactions on Intelligent Transportation Systems. 2017; **18**(1):49-58. DOI: 10.1109/TITS. 2016.2521866

[9] Wang S, Minku L, Yao X. A systematic study of online class imbalance learning with concept drift. IEEE Transactions on Neural Networks and Learning Systems. 2018;**29**(10): 4802-4821. DOI: 10.1109/ TNNLS.2017.2771290

[10] Zhang KP, Jiang B, Tao G, Chen FY. MIMO evolution model based coupled fault estimation and adaptive control with high speed train applications. IEEE Transactions on Control Systems Technology. 2018;**26**(5):1552-1566. DOI: 10.1109/TCST.2017.2735360

[11] Nguyen V, Wang DW, Seshadrinath J, Ukil K, Krishna MS, Nadarajan S, et al. A method for incipient interturn fault detection and severity estimation of induction motors under inherent asymmetry and voltage imbalance. IEEE Transactions on Transportation Electrification. 2017; **3**(3):703-715. DOI: 10.1109/TTE. 2017.2726351

[12] Pandey VK, Kar I, Mahanta C. Controller design for a class of nonlinear MIMO coupled system using multiple models and second level adaptation. IEEE Transactions on Transportation Electrification. 2017;**69**:256-272. DOI: 10.1016/j. jsatra2017.05.005

[13] Bethoux O, Laboure E, Remy G, Berthelot E. Real-time optimal control of a 3-phase PMSM in 2-phase degraded mode. IEEE Transactions on Vehicular Technology. 2017;**66**(3):2044-2052. DOI: 10.1109/TVT.2016.2583662

[14] Zhang KP, Jiang B, Chen FY. Multiple-model-based diagnosis of multiple faults with high-speed train applications using second-level adaptation. IEEE Transactions on Industrial Electronics. 2021;**68**(7): 6257-6266. DOI: 10.1109/TIE.2020. 2994867

[15] Gao ZW, Liu XX, Chen MZQ. Unknown input observer-based robust fault estimation for systems corrupted by partially decoupled disturbances. IEEE Transactions on Industrial Electronics. 2016;**63**(4):2537-2547. DOI: 10.1109/2015.2497201

[16] Yang ML, Deng C, Nie FP. Adaptive-weighting discriminative regression for multi-view classification. Pattern Recognition. 2019;**88**:236-245. DOI: 10.1016/j.patcog.2018.11.015

[17] Mustafa MO, Nikolakopoulous G, Gustafsson T, Kominiak D. A fault detection scheme based on minimum identified uncertainty bounds violation for broken rotor bars in induction motors. Control Engineering Practice. 2016;**48**:63-77. DOI: 10.1016/ j.conengprac.2015.12.008

[18] Davies DL, Bouldin DW. Cluster separation measure. IEEE Transactions on Pattern Analysis and Machine Intelligence. 1979;**1**(2):224-227